VII International Conference on Particle-Based Methods
PARTICLES 2021
P. Wriggers, M. Bischoff, E. Oñate, M. Bischoff, A. Düster & T. Zohdi (Eds)

NUMERICS OF DISCRETE ELEMENT SIMULATIONS IN MILLI-G ENVIRONMENTS: CHALLENGES AND SOLUTIONS

Felix Buchele[1,2], Roy Lichtenheldt[2] and Leon Stubbig[2]

[1] Department of Mechanical Engineering
University of Applied Sciences Kempten
Bahnhofstr. 61, 87435 Kempten, Germany
e-mail: buchelefelix@gmail.com, www.hs-kempten.de/en/

[2] Institute of System Dynamics and Control
German Aerospace Center (DLR)
Münchener Straße 20, 82234 Weßling, Germany
e-mail: roy.lichtenheldt@dlr.de, leon.stubbig@dlr.de, www.dlr.de/sr/

Key words: Phobos, DEM, Numerical Precision, MMX, Locomotion, Microgravity

Abstract. JAXA scheduled a sample return mission to the martian moon Phobos, which is expected to launch in 2024. This mission features a small rover, jointly developed by DLR and CNES, which will scout the landing site of the sampling spacecraft. One of the main challenges the rover will have to face during the mission is the vastly unknown regolith surface of Phobos. Previous exploration missions, like the Mars Exploration Rover missions of NASA, showed, that a rover getting stuck in loose regolith poses a huge threat to the success of planetary exploration missions. To prevent this, DEM simulations are used to optimize the rover's wheel geometry for Phobos' surface.

The DLR framework for such simulations is *partsival*, a collision-based particle and many-body simulation tool for GPUs. Since *partsival* was programmed with simulations in Lunar, Martian, or Earth environments in mind, the framework has to be adapted for milli-g environments. Without any adaptations, the simulation results show severe scattering and physically unrealistic behavior. These issues can be traced back to numerical problems related to the introduction of microgravity. The low gravity requires very slow movement of the rover wheel, resulting in a very long simulation duration and therefore the necessity to compute billions of time steps. Error propagation is thus strongly favored. Furthermore, while simulations in Earth or Lunar environments can be conducted using *single-precision*, milli-g environments showed to require *double-precision* computations. This is due to the gravity influencing many (but not all) parameters of *partsival*'s physics model, resulting in changes by orders of magnitude and loss of significance errors.

partsival can be adapted to milli-g environments by adapting the macroscopic soil stiffness to allow for larger time steps while at the same time increasing the numerical precision. Thus, deterministic results can be computed while maintaining fast, efficient computation.

1 INTRODUCTION

After several successful manned and unmanned moon landings, the focus of space exploration shifted towards Mars and its moons Phobos and Deimos. Along with the search for traces of life on Mars, the exploration of the martian system also promises deeper insight into the formation processes of our solar system. Furthermore, smaller celestial bodies like asteroids or comets were the object of several exploration missions of the last decade. Successful missions like the *Hayabusa 1* [27] and *Hayabusa 2* missions of the Japan Aerospace Exploration Agency (JAXA), the *NEAR Shoemaker* mission [26] of the National Aeronautics and Space Administration (NASA) or the *Rosetta* mission [3] of the European Space Agency (ESA) intensified the pretensions to explore such celestial bodies [24].

1.1 The MMX mission

The for 2024 scheduled *Martian Moons eXploration* (MMX) mission of JAXA combines both, small celestial body exploration and the exploration of the martian system. This mission aims to study the martian moons Phobos and Deimos. While Deimos will only be observed remotely, the MMX spacecraft is supposed to land on Phobos to sample the moon's surface. Since MMX is a sample return mission, the spacecraft will leave Phobos and return the regolith samples to earth. [25] In advance of the sampling spacecraft's landing, a rover will be deployed to the surface of Phobos. This rover is jointly developed by the German Aerospace Agency (DLR) and the French National Centre for Space Studies (CNES). It assumes several tasks. Firstly, the rover allows for in situ studies of the Phobos regolith. That's why the rover features several scientific instruments like a Raman spectrometer, a gravimeter, a radiometer, and several cameras. [21, 23, 2]

Secondly, the rover is supposed to secure the landing of the sample return spacecraft. After being dropped at the planned landing site in advance of the spacecraft's landing, the rover can scout the surroundings. The rover will examine the Phobos regolith in order to determine its properties. One of the greatest threats to the spacecraft landing on Phobos, namely sinking into loose regolith or tipping over during the landing, can be assessed by thoroughly scouting the landing site. [21, 2, 18]

The MMX mission constitutes the first mission of its kind which involves the deployment of a wheeled rover in milli-g environment. No wheeled rover has ever been deployed before in a comparably low gravitational environment. Therefore, the locomotion capabilities of the rover cannot be foreseen yet and have to be determined beforehand. In the course of rover missions to other celestial bodies, the locomotion capabilities of rovers were often determined by experiment. Since this is no longer appropriate in milli-g environments, DEM simulations will be used to evaluate the rover's tractive performance [4, 5].

1.2 Environmental challenges on Phobos

The vastly unknown regolith surface of Phobos poses a major threat to the mission's success. Despite Phobos has been the aim of several exploration missions, in-depth examination of Phobos hasn't been successful yet. The Soviet *Fobos-Grunt* mission [15]

and the Russian *Phobos 1* and *Phobos 2* missions [19], which also targeted Phobos, failed and never managed to reach it's surface. Some surface properties can be assumed by remote sensing, though. Phobos is believed to have a several meters thick regolith layer [9] with grains with a diameter ranging from 30 µm up to a few centimeters [1]. The friction angle is assumed to be around 20° and the POISSON ratio of the Phobos regolith is believed to be around 0.15 [17]. Whether the soil is cohesive or not is not clear yet. The cohesive strength of the Phobos regolith is believed to be between 100 Pa and 1000 Pa [20].

Also challenging for the rover as well as for the simulation framework is the gravitational regime on Phobos. Roving on Phobos with its low gravity is likely an endeavor close to the limits where wheeled rover locomotion still makes sense. If the rover drives too fast, it might even lift off from Phobos' surface. [5] The surface gravity of Phobos varies strongly due to the irregular, elliptic form of the moon. The perceived gravity on Phobos is furthermore composed of different forces. Due to Phobos' proximity to Mars, the martian gravity also influences the gravitational regime by its tidal forces. Also, the centrifugal force, resulting from Phobos' rotation, affects the perceived Phobos gravity. Therefore, the gravity regime on Phobos should rather be called effective gravity, which includes gravity, tidal and centrifugal forces. The effective gravity on Phobos' surface fluctuates roughly between $3 \times 10^{-3}\,\mathrm{m\,s^{-2}}$ to $6.8 \times 10^{-3}\,\mathrm{m\,s^{-2}}$. [9, 22]

2 Simulation Framework

Since the experimental evaluation of the rover wheel's traction is not possible, a numerical simulation approach is chosen to assess the tractive performance. The software used to perform the simulations is *partsival*, a collision-based Discrete Element Method (DEM) and many-body simulation tool, developed by DLR. *partsival* is a GPU-based simulation framework with an excellent computation performance, especially with huge numbers of particles, by making use of thousands of GPU shaders in parallel [13].

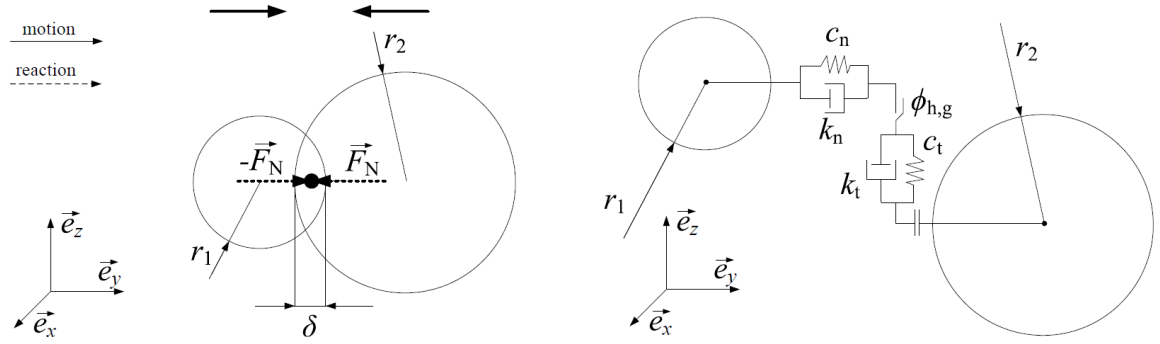

Figure 1: Soft particle contact (left) and contact model for normal and tangential contacts (right) [14]

partsival uses a rigid body contact model to reproduce the interactions of soil particles. Since complex grains are discretized as simple spheres, *partsival* features an advanced friction model which can depict positive locking and friction effects of real grains. The interaction between two particles is modeled as a soft contact. This means, that two

particles contacting each other lead to an overlap $\vec{\delta}$ between them. The contact is made as soon as the distance between the particles is smaller than the sum of the particle radii r_1 and r_2 [14]. This relationship is shown in Figure 1.

Normal contact forces $\vec{F}_\mathrm{N}$ between two particles n and m are calculated as HERTZian contacts. The contact damping forces are implemented according to LEHR as mass-scaled damping forces with the damping coefficient k^{nm}_{Nmin}. The contact in normal direction in case of overlap evaluates therefore to:

$$\vec{F}^{nm}_\mathrm{N} = \left(\frac{2E}{3(1-\nu^2)} \sqrt{r^{nm}_\mathrm{C} |\vec{\delta}^{nm}|^3} \right) \vec{n}^n_\mathrm{c} + k^{nm}_{\mathrm{Nmin}} \dot{\vec{\delta}}^{nm}; \quad \forall \vec{\delta}^{nm} \neq 0 \tag{1}$$

with the mean radius r_C between the two particles, the contact normal for each particle $\vec{n}^n_\mathrm{c}$, the YOUNG's Modulus E, and the POISSON's ratio v. [14, 10]

The tangential contact model features stick-slip friction with a regularized COULOMB friction model. The regularization is implemented to distinguish between stick and slip friction and is performed by using a KELVIN element. The force $\vec{F}^{nm}_\mathrm{cT}$ of the KELVIN element evaluates to:

$$\vec{F}^{nm}_\mathrm{cT} = c^{nm}_\mathrm{T} \cdot \vec{\delta}^{nm}_\mathrm{T} \cdot sign \left(\vec{\delta}^{nm}_\mathrm{T} \cdot \dot{\vec{\delta}}^{nm}_\mathrm{T} \right) + k^{nm}_\mathrm{T} \cdot \dot{\vec{\delta}}^{nm}_\mathrm{T} \tag{2}$$

with the tangential stiffness c^{nm}_T, the damping coefficient k^{nm}_T and the displacement $\vec{\delta}^{nm}_\mathrm{T}$. The total tangential force is evaluated depending on the KELVIN element's force and yields:

$$\vec{F}^{nm}_\mathrm{T} = \begin{cases} \vec{F}^{nm}_\mathrm{cT}; & \forall \, |\vec{F}^{nm}_\mathrm{cT}| \leq |\vec{F}^{nm}_\mathrm{N}| \cdot \tan(\phi_\mathrm{h}) \ \wedge \ |\dot{\vec{\delta}}^{nm}_\mathrm{T}| \leq v^{nm}_{\mathrm{Tmin}} \\ |\vec{F}^{nm}_\mathrm{N}| \cdot \tan(\phi_\mathrm{g}) \cdot \left(\dot{\vec{\delta}}^{nm}_\mathrm{T} \right)_0; & \forall \, |\vec{F}^{nm}_\mathrm{cT}| > |\vec{F}^{nm}_\mathrm{N}| \cdot \tan(\phi_\mathrm{h}) \ \vee \ |\dot{\vec{\delta}}^{nm}_\mathrm{T}| > v^{nm}_{\mathrm{Tmin}} \end{cases} \tag{3}$$

whereby the tangential velocity $\dot{\vec{\delta}}^{nm}_\mathrm{T}$ and the MOHR-COULOMB yield criterion with the sticking friction angle ϕ_h are used to differ between stick and slip friction. If the tangential velocity is lower than v^{nm}_{Tmin} and if the yield criterion is not met, the KELVIN element defines the tangential force $\vec{F}^{nm}_\mathrm{T}$. Otherwise, if either the MOHR-COULOMB yield criterion is met or $\dot{\vec{\delta}}^{nm}_\mathrm{T}$ exceeds v^{nm}_{Tmin}, slipping friction with the friction angle ϕ_g occurs. [14, 10]

Based on *partsival*'s contact model, NEWTON's equations of motion and momentum can be evaluated for each particle. Following the mechanical equilibrium, the sum of all forces and moments, $\sum_{j=0}^{n} \vec{F}^{ij}_\mathrm{C}$ and $\sum_{j=0}^{n} \vec{T}^{ij}_\mathrm{C}$ respectively yields:

$$m^i \ddot{\vec{x}}^{\,i} = \sum_{j=0}^{n} \vec{F}^{ij}_\mathrm{C} \tag{4}$$

$$\vec{I}^{\,i} \cdot \dot{\vec{\omega}}^i + \vec{\omega}^i \times \vec{I}^{\,i} \cdot \vec{\omega}^i = \sum_{j=0}^{n} \vec{T}^{ij}_\mathrm{C} \tag{5}$$

where each particle i is evaluated depending on mass m^i, inertia $\vec{I}^{\,i}$ and angular velocity $\vec{\omega}(t)^i$. $\vec{x}(t)^i$, $\dot{\vec{x}}(t)^i$ and $\ddot{\vec{x}}(t)^i$ are the particle position, velocity and acceleration respectively. [13]

Subsequently, an integration scheme can be applied on NEWTON's equations, which allows the computation of future system states. *partsival* uses a semi-implicit integration scheme, namely the LICHTENHELDT-jolt-BEEMAN scheme, which is described in [12]. This multi-step scheme allows the transition from system state x_0 at the time t_0 to x_1 at the time t_1 over the intermediate steps κ_1 to κ_3. In contrast to purely implicit schemes, the intermediate steps are evaluated using an explicit estimate where the particle jolt is assumed to be zero. This yields:

$$\frac{d^3\vec{x}}{dt^3}(t) = \left.\frac{\dddot{\vec{x}}}{dt}\right|_{(t-\Delta t)}^{t} = const \tag{6}$$

The main advantage of this scheme is, that it is not necessary anymore to calculate the right-hand evaluations of NEWTON's equations for each step κ. Those evaluations are very time-critical, especially because they usually require a reevaluation of neighborhood search and contact forces. Thus, the LICHTENHELDT-jolt-BEEMAN scheme enables a precise and time-saving integration [12]. The remaining integration error $\mathcal{O}(h)$ is used to improve the integration precision. *partsival* generally uses a variable time step size, defined by a minimal and maximal time step size and by the integration error tolerance. If the integration error $\mathcal{O}(h)$ exceeds the previously set tolerance value, a PID controller changes the time step size accordingly, to keep the integration error within tolerable bounds.

Regarding numerics, *partsival* has so far usually used *single-precision* computation for rover wheel simulations. Even though rather uncommon in scientific applications, *single-precision* has proven to deliver results with sufficient precision [13]. Figure 2 shows the results of two identical single wheel experiments with the traveled distance over time in the left plot and the wheel sinkage in the right plot respectively. The simulation was performed using *partsival* and *single-precision* computation. Especially regarding the wheel sinkage, it can be seen, that minor result deviation occurs. But regarding the wheel's traveled distance, almost no deviation is visible. Therefore, the simulation results for wheel slip, velocity, and travel distance can be seen as deterministic. If the wheel's sinkage is evaluated as average sinkage, the deviations almost completely cancel out themselves. The average sinkage can therefore also be considered as deterministic. We call this context macroscopic determinism. While individual particle positions or even the wheel's position at a certain point of time may differ in repeated simulation runs and are therefore non-deterministic, the quantities of interest, namely wheel travel distance, slip, velocity, and average sinkage, are deterministic and match with experimental findings [16]. The example furthermore demonstrates that *single-precision* computation can be suitable for wheel-soil-interaction simulations.

3 NUMERICAL CHALLENGES

While *partsival* performs very well with gravitational forces ranging from Earth to Moon gravity (see Fig. 2), it has not been tested before with extremely low gravitational forces like those occurring on Phobos. Therefore, the simulation framework has to be tested regarding its capabilities to simulate milli-g environments. The change in gravitational

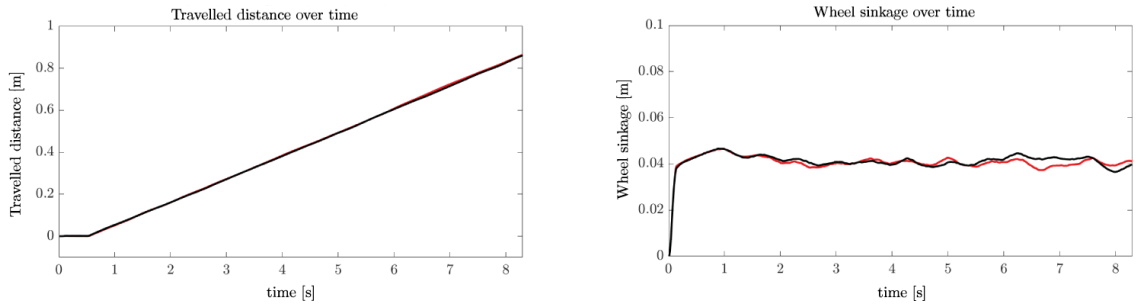

Figure 2: Results of a wheel experiment, carried out twice under earth gravity and in *single-precision*

acceleration leads to a change of magnitude of many (but not all) parameters of *partsival*'s physics model. By examining the equations 1 to 3 we can deduce for example, that particle overlap $\vec{\delta}$ and overlapping velocity $\dot{\vec{\delta}}$ will shrink with lower gravitational acceleration. This is because the forces acting on single particles and particles beneath the wheel will be by magnitudes lower due to less gravitational acceleration and less weight force exerted by the rover wheel. However, parameters like YOUNG's modulus E, POISSON's ratio v or the damping coefficient k don't depend on and don't change with gravity.

Furthermore, the by magnitudes lower forces acting on particles and wheel also directly impact time integration. The change in magnitudes to the overall acting forces within the simulation also influences the overall simulation error. Assuming that the percentage error remains unchanged by the change in gravity, the absolute error changes linearly with gravity. Since the integration time step size h is derived from a tolerance, based on the absolute error, the gravitational acceleration directly interferes with *partsival*'s time integration. In the specific case with Phobos gravity, the sum of all forces acting on particles and wheel is of the same order of magnitude as the integrator's tolerance.

In addition and due to the reduced gravity on Phobos, the rover will have to move on Phobos far slower than any other rover in higher gravity environments. The MMX rover will explore Phobos with a maximum velocity of approx. $2.5\,\mathrm{cm\,s^{-1}}$ [4, 5]. When traveling faster, the rover is at risk to lift off due to the low gravity on Phobos. Since DEM wheel simulations need to settle in, the simulation of at least one to two wheel revolutions is required. Thus, the low angular velocity of the rover wheel leads to a massive increase in simulation time. While the experiment under earth gravity, pictured in Figure 2, requires less than 10 s of simulation time, the wheel experiments for the MMX mission require more than 60 s of simulation time. The increasing simulation time increases the number of time steps and therefore favors the accumulation of rounding errors and integration errors.

As a result of the above-mentioned issues, when repeating the exact same simulation run several times, the simulation results are massively scattered. The slip of a wheel for example can vary between approx. 20 % and 80 %. Figure 3 shows the results of 20 identical simulations, that are heavily scattered and therefore proofs impressively the need for adaptations to the simulation framework when changing the gravitational acceleration.

The Figure shows the traveled distance of several wheels and their respective wheel sinkage over the simulation time. Wheel geometry, contact model, integrator settings, wheel

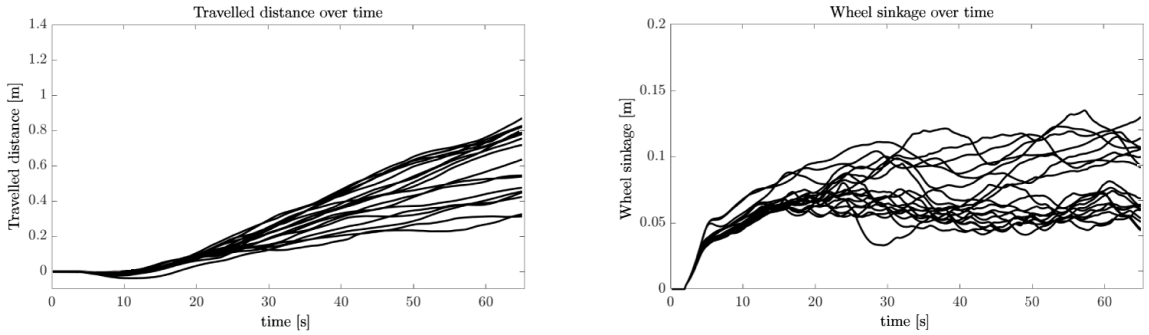

Figure 3: Result scattering after performing 20 identical simulations with *partsival* in *single-precision*

angular velocity, and initial particle positions have not been altered between simulation runs. It can be seen, that the simulation results start to diverge after approx. 10 s and scatter even further with increasing simulation time. Macroscopic determinism is clearly not given anymore. In addition to the result deviation, the wheels also perform way worse than anticipated. We attribute this to numerical errors within the determination of stick or slip friction (see equations 2 and 3). If particles are oscillating with high frequencies and low amplitudes, stick friction cannot occur. The relative velocity between particles n and m, $\dot{\vec{\delta}}_{\mathrm{T}}^{nm}$ is therefore always higher than the reference velocity v_{Tmin}^{nm}, leading to less shear strength of the soil.

The simulation result deviation is a well-known issue that arises when making use of massively parallelized computations in combination with floating-point arithmetics [8]. With said constellation, the commutative law of mathematics is not applicable anymore. A floating-point number will be stored in memory as a combination of exponent and mantissa. The number x can therefore be described with $x = m \times b^e$, where m is the mantissa, b is the base and e is the exponent [7]. This enables the efficient storage of very large and very small numbers within a relatively small bit width. But on the other hand, it leads to rounding errors, when overflow occurs, meaning that not all significant digits can be stored anymore. Usually, this overflow occurs within the mantissa [8].

The result scattering, originating from massively parallelized computation in combination with IEEE floating-point algorithms, can be illustrated by an example. To simplify the example, *half precision* computation will be applied. We're totaling 10, 0.003 and 0.001 in binary. By changing the order of the summands, the result changes as well:

$$\begin{aligned} &0.003 + 0.001 + 10.00 = && 0.00110.1000100101 + 0.00101.0000011001 + 0.10010.0100000000 = \\ &0.004 + 10.00 \approx 10.01 && 0.00111.0000011001 + 0.10010.0100000000 \approx 0.10010.0100000001 \end{aligned} \tag{7}$$

$$\begin{aligned} &0.003 + 10.00 + 0.001 \approx && 0.00110.1000100101 + 0.10010.0100000000 + 0.00101.0000011001 \approx \\ &10.00 + 0.001 \approx 10.00 && 0.10010.0100000000 + 0.00101.0000011001 \approx 0.10010.0100000000 \end{aligned} \tag{8}$$

to improve intelligibility, the left column of both equations shows the decimal equivalent of the binary calculations on the right. For better legibility, sign bit, exponent, and mantissa

are separated from each other in this order by a dot. Both summation orders not only yield false results but also yield different results. This is because rounding only occurs once with the first summation order and twice with the second summation order. The example also shows, that such errors always occur within the least significant bit.

partsival and comparable simulation frameworks are prone to such errors since there are huge sums that have to be calculated. Since the soil simulation can consist of several hundred thousand particles, the accumulation of forces acting on the wheel can consist of several thousand summands. Also, the NEWTONian sum of forces and moments (see equation 4 and 5) can grow rather large. Based on this first minor result deviation that might occur here, error propagation can lead to a massive increase of the deviation.

The emergence of errors in a simulation framework like *partsival* can be described depending on the time step size h using LANDAU NOTATION:

$$\Delta = \mathcal{O}(h) + \mathcal{O}(\varepsilon/h) \tag{9}$$

where the overall error Δ is composed of the integration error $\mathcal{O}(h)$ and the numerical rounding error $\mathcal{O}(\varepsilon/h)$. While a smaller time step size reduces the integration error, the rounding errors increase [6]. This is because a smaller time step size also results in more time steps that require computation, which favors error propagation of rounding errors. This is clearly visible in Figure 3, where errors only emerge after a certain amount of simulation time, proving that the simulation duration is a factor, which strongly affects error propagation. In the specific example, noticeable result scattering starts to emerge at about 20 s of simulation time and grows ever further. Following equation 9, the overall simulation error Δ can be reduced by minimizing integration error and numerical errors.

4 SOLUTIONS

To regain macroscopic determinism for milli-g simulations, error propagation and result scattering must be minimized. The means to do so and to reduce the overall simulation error Δ, are given from the simulation error description following LANDAU. Both, numerical rounding error and integration error depend on the time step size h. But since both errors scale contrary with time step size, there must exist a time step size h, where $\Delta = \mathcal{O}(h) + \mathcal{O}(\varepsilon/h) = min$. The influence of the time step size on the simulation error Δ is therefore rather limited [6]. To further reduce the simulation error, the numerical errors and integration errors have to be targeted individually.

4.1 Minimizing $\mathcal{O}(\varepsilon/h)$

The easiest way to minimize numerical errors and to reduce result scattering is by increasing the numerical precision. As mentioned before, *partsival* delivers exact results in higher gravity environments using *single-precision* computation. By raising the precision to *double-precision*, the magnitude of numerical errors changes immensely. Since the numerical errors discussed earlier only affect the least significant bits, the overall error is decreased dramatically. By increasing the numerical precision from *single* to *double*, the mantissa bit width more than doubles. The erroneous bit shifts therefore by 29 bits [7].

In decimal numbers, this corresponds to a shift of approx. 8 decimal digits and therefore reduces simulation errors by a factor greater than 1×10^7.

Of course, error propagation is still effective. But since errors appear in lower magnitude, error propagation is also reduced. Figure 4 proves this. Here we can see - similarly to Figure 3 - the simulation results of 20 identical wheel experiments. In contrast to the *single-precision* simulation results, the *double-precision* results show almost no scatter. Macroscopic determinism can therefore be regained by increasing the numerical precision. The simulation results also show that the differentiation between stick and slip friction works again. Due to reduced numerical errors, particle oscillation can be prevented as well, leading to a reasonable soil shear strength and therefore to realistic wheel sinkage.

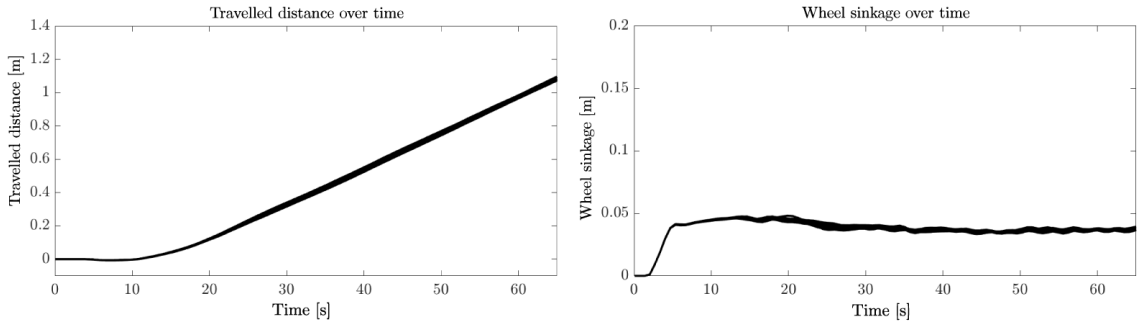

Figure 4: Result scattering after performing 20 identical simulations with *partsival* in *double-precision*

4.2 Minimizing $\mathcal{O}(h)$

After eliminating the main reasons for result scattering and numerical errors by increasing numerical precision, an optimal time step size h can be defined to minimize the integration error. Previous research showed that *partsival* requires a time step size of 1×10^{-5} s when performing wheel experiments in Earth, Moon or Mars gravity [4]. By reducing the gravitational acceleration acting on wheel and soil, the time step size can be reduced as well. We found, that the simulations are still stable and deliver valid results with time step sizes as low as 5×10^{-4} s.

Tests with time step sizes varying between 1×10^{-5} s and 1×10^{-6} s also showed no noticeable improvements regarding result scattering, compared to the lowest possible, stable time step sizes [4]. When applying even higher time step sizes, numerical stability is not given anymore. This leads to a violation of the principle of conservation of energy and ultimately to an "explosion" of the simulation, where particles accelerate randomly. Unlike the result scattering, this kind of error can be witnessed in any gravitational environment and is not linked to simulation gravity [4].

Also in contrary to the result scattering, such numerical instabilities are easy to recognize and easy to avoid. In the given case, we increased the time step size incrementally, until numerical instabilities occurred. The highest stable time step size has proven to be optimal in terms of simulation time and numerical errors. To completely avoid numerical instabilities, we applied a safety margin to the maximal time step size.

5 NUMERICAL STABILITY

After applying changes to the computation framework of *partsival* by increasing its numerical precision and after determining an adequate time step size, where the overall simulation error Δ is minimal, we apply a further method to increase the numerical stability of the simulations.

As introduced before in the equations 1 - 3, *partsival* uses a soft contact model to determine contact forces between particles. The contact model's particle stiffness is however not based on the granular material's stiffness. It is rather defined as a macroscopic stiffness, describing the behavior of grain agglomerates, when force is exerted on them. Since the rover's weight on Phobos depends on surface gravity, the forces exerted on Phobos' soil are orders of magnitude smaller, compared to the forces that would be exerted when simulating higher gravity environments, such as Earth or Mars.

Therefore, the macroscopic contact stiffness can be adapted to Phobos' low gravity environment. To do so, we apply an equation developed by LICHTENHELDT in [11]:

$$E_{\mathrm{mP}} \geq z_{\mathrm{h}} \frac{|3\vec{p} + z_{\mathrm{h}} \cdot \rho_{\mathrm{p}} \cdot \vec{g}|}{3|\vec{u}| \cdot r} \tag{10}$$

where the macroscopic particle contact stiffness E_{mP} is derived from the soil height z_{h} of the simulation environment, the pressure $\vec{p}$ exerted on the ground by the rover wheels, the overlapping factor $\vec{u}$, the particle radius r and the deadweight force of the soil, calculated by its height z_{h}, the particle density ρ_{p} and gravity $\vec{g}$.

Based on this equation, we can significantly reduce macroscopic contact stiffness. This enables a suitable overlap between two contacting particles and increases numerical stability of the simulation without the results deviating from reality [4]. Also, the adapted damping reduces particle oscillation, thus avoiding erroneous computations of stick/slip friction, which ultimately allows for even larger time step sizes in the range of 2×10^{-4} s.

6 CONCLUSIONS AND OUTLOOK

The initial problem, simulation result scattering and result deviation can be resolved by applying several adaptations to the simulation framework. After proving, that the numerical issues were caused by the massive reduction of the gravitational acceleration, we were able to track down, where exactly the low gravity environment interferes with the previously perfectly working simulation framework. Based on those findings, we were able to develop methods to reduce result deviation and scatter.

The by far easiest way to reduce result scatter and deviation proved to be an increased numerical precision. Unfortunately, computation duration increased due to the higher numerical precision. Therefore we plan to implement a mixed-precision option, where only those computations that are vulnerable to numerical errors will be computed using *double-precision*. Whenever *single-precision* is sufficient, we plan to stick with it.

After having dealt with result scattering, we turned towards the integration scheme. The gravitational environment on Phobos proved to be otherwise numerically good-natured. Due to the low forces exerted on wheel and soil and due to the slow movement of the

rover's wheel, the integration time step could be raised significantly. Even though the required simulation time for our experiments was more than six times the simulation time of comparable experiments under Earth or Mars gravity, we achieved comparable computation times. We were able to perform wheel simulations with > 200.000 particles and over 60 s simulation in time in less than 24 h, using Nvidia Tesla GPUs. Finally, the simulation stability was greatly improved by lowering the macroscopic particle stiffness for soft normal contacts, which allowed for even larger time steps and thus further reducing computation time.

Summarized, we managed to adapt *partsival*, a DEM framework that was never developed with milli-g environments in mind to the extremely low gravitational regime of Phobos. By doing so, we managed to maintain *partsival*'s macroscopic determinism while at the same time achieving relatively low computation times. Thus, the optimization campaign could be conducted as planned. Rover wheel traction in milli-g on Phobos could be assessed using *partsival* with the adaptations presented in this paper, leading to an optimized rover wheel design [5].

REFERENCES

[1] A. T. Basilevsky. et al. The surface geology and geomorphology of phobos. *Planetary and Space Science*, 102:95–118, 2014.

[2] J. Bertrand. et al. Roving on phobos: Challenges of the mmx rover for space robotics. In *15th Symposium on Advanced Space Technologies in Robotics and Automation*, 2019.

[3] J. Biele. et al. The landing(s) of philae and inferences about comet surface mechanical properties. *Science*, 349(6247), 2015.

[4] F. Buchele. *Optimierung der Traktion eines planetaren Rovers mit der Diskreten Elemente Methode*. Master's thesis, University of Applied Sciences Kempten, Kempten, 2020.

[5] F. Buchele and R. Lichtenheldt. Multi-parameter rover wheel and grouser optimization for deployment in phobos milli-g environment. In *International Symposium on Artificial Intelligence, Robotics and Automation in Space (i-SAIRAS)*, 2020.

[6] S. Gerlach. *Computerphysik*. Springer Verlag, Berlin, Heidelberg, 2019.

[7] Institute of Electrical and Electronics Engineers. *IEEE Standard for Floating-Point Arithmetic: IEEE Std 754-2019 (Revision of IEEE 754-2008)*. IEEE Standards Association, New Jersey, 2019.

[8] E. Kadric, P. Gurniak, and A. DeHon. Accurate parallel floating-point accumulation. *IEEE Transactions on Computers*, 65(11):3224–3238, 2016.

[9] R. O. Kuzmin, T. V. Shingareva, and E. V. Zabalueva. An engineering model for the phobos surface. *Solar System Research*, 37(4):266–281, 2003.

[10] R. Lichtenheldt. A novel systematic method to estimate the contact parameters of particles in discrete element simulations of soil. In *4th International Conference on Particle-based Methods - Particles*, pages 430–441, 2015.

[11] R. Lichtenheldt. *Lokomotorische Interaktion planetarer Explorationssysteme mit weichen Sandböden*. Doctoral thesis, Technische Universität Ilmenau, 2016.

[12] R. Lichtenheldt. A stable, implicit time integration scheme for discrete element method and contact problems in dynamics. In *5th International Conference on Particle-based Methods - Particles*, pages 297–308, 2017.

[13] R. Lichtenheldt. et al. partsival - collision-based particle and many-body simulations on gpus for planetary exploration systems. In *The 5th Joint International Conference on Multibody System Dynamics*, 2018.

[14] R. Lichtenheldt and B. Schäfer. Planetary rover locomotion on soft granular soils - efficient adaption of the rolling behaviour of nonspherical grains for discrete element simulations. In *3rd International Conference on Particle-Based Methods*, pages 807–818, 2013.

[15] M. Marov. et al. Phobos-grunt: Russian sample return mission. *Advances in Space Research*, 33(12):2276–2280, 2004.

[16] S. Ono. *Evaluation of Planetary Rover Wheel Performance on Sloped Loose Soil Based on Discrete Element Method*. Master's thesis, Tohoku University, Sendai, 2019.

[17] C. M. Pieters. et al. Composition of surface materials on the moons of mars. *Planetary and Space Science*, 102:144–151, 2014.

[18] D. J. Rodgers. et al. Methodology for finding and evaluating safe landing sites on small bodies. *Planetary and Space Science*, 134:71–81, 2016.

[19] R. Z. Sagdeev and A. V. Zakharov. Brief history of the phobos mission. *Nature*, 341(6243):581–585, 1989.

[20] D. J. Scheeres. et al. Scaling forces to asteroid surfaces: The role of cohesion. *Icarus*, 210(2):968–984, 2010.

[21] S. Tardivel and C. Lange. The mmx rover: An innovative design enabling phobos in-situ exploration. In *13th IAA Low-Cost Planetary Missions Conference*, 2019.

[22] P. C. Thomas. Gravity, tides, and topography on small satellites and asteroids: Application to surface features of the martian satellites. *Icarus*, 105(2):326–344, 1993.

[23] S. Ulamec. et al. A rover for the jaxa mmx mission to phobos. In *70th International Astronautical Congress*, 2019.

[24] S. Ulamec and J. Biele. Surface elements and landing strategies for small bodies missions – philae and beyond. *Advances in Space Research*, 44(7):847–858, 2009.

[25] T. Usui. et al. The importance of phobos sample return for unterstanding the mars-moon system. *Space Science Reviews*, 216(49):480–488, 2020.

[26] J. Veverka. et al. The landing of the near-shoemaker spacecraft on asteroid 433 eros. *Nature*, 413(6854):390–393, 2001.

[27] H. Yano. et al. Touchdown of the hayabusa spacecraft at the muses sea on itokawa. *Science*, 312(5778):1350–1353, 2006.